Structural and Modal Analysis of the L75 Rocket Engine Turbine Disk at Operating Conditions

Daniel Bourdon[1], Carlos Souto[2], Ronaldo C. Reis[3], Daniel F. Sias[4]

[1] *Institute of Aeronautical and Space, Department of Science and Aerospace Technology, São José dos Campos, São Paulo /SP, Brazil.*
daniel.bourdon@ga.ita.br, danielbourdon3@gmail.com
[2] *Division of Integration and Tests, Institute of Aeronautical and Space, Department of Science and Aerospace Technology, São José dos Campos, São Paulo /SP, Brazil.*
carlos.dandrade.souto@gmail.com
[3] *Institute of Aeronautical and Space, Department of Science and Aerospace Technology, São José dos Campos, São Paulo /SP, Brazil.*
chavesrcr@fab.mil.br
[4] *Wikki Brasil Consultoria em Engenharia LTDA, Parque Tecnológico, São José dos Campos, São Paulo/SP, Brazil*
daniel.sias@wikki.com.br

Abstract. The development of a biofuel turbopump was initiated at the Institute of Aeronautics and Space (IAE) in 2013 under Brazilian Space Agency (AEB) support and in the context of the L75 Rocket Engine project. The turbopump is composed by an oxidizer pump, a fuel pump and a supersonic-flow single-stage turbine. Due to the high rotational speed and high temperature it is subjected for, the turbine is considered one of the most critical components of the rocket engine. In this study, an appropriate structural and modal FEM analysis of the turbine rotor is performed. Temperature and rotational influence on material properties, the temperature gradient, rotational speed and gas pressure distribution effects are considered. The main failure modes of the L75 turbine are elastic deformation, plastic deformation, high-cycle fatigue and low-cycle fatigue. It was not considered creep as a failure mode due to the short life the turbine is designed for. Therefore, a thermo-elastic and a modal analysis of the turbine rotor are performed using a FEM commercial software, considering actual operation environment conditions. The results are presented graphically, a discussion is carried out and a design modification is proposed in order to reach the turbine requirements.

Keywords: FEM structural analysis, supersonic-flow turbine, turbopump, L75 rocket engine.

1 Introduction

The development of a biofuel turbopump was initiated at the Institute of Aeronautics and Space (IAE) in 2013 under Brazilian Space Agency (AEB) support and in the context of the L75 Rocket Engine project, as Almeida [1]. The development process includes the design, manufacturing and testing of the turbopump at components and assembly levels. The turbopump is composed by an oxidizer pump, a fuel pump and an axial-flow turbine, as shown in the Fig.1, as defined by Zink [2]. The supersonic-flow single-stage partial-admission turbine is driven by the combustion gases from a bipropellant gas generator using oxygen and ethanol. Due to the high rotational speed and high temperature the turbine is subjected for, it is considered one of the most critical components of the engine, as Boyce [3] and Giampaolo [4].

The main failure modes of the L75 turbine are elastic deformation, plastic deformation, high-cycle fatigue, and low-cycle fatigue. Stress-rupture (creep) was not considered as a failure mode due to the short life the turbine

is designed for (about one hour), as defined in Almeida [1] and Pfuetzenreuter [5]. The turbine rotor expansion is a critical parameter as the blade tip gap is strongly related to the turbine performance. The high- and low-cycle fatigue are failure modes directly related to the vibration and thermal gradient stress, respectively, as Sims [6].

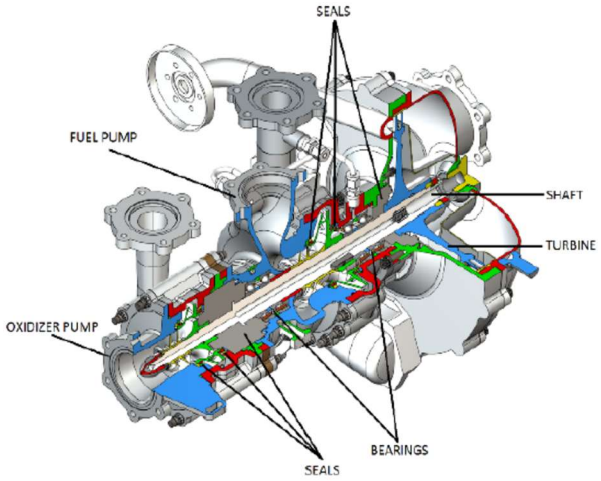

Figure 1. L75 Turbopump Assembly.

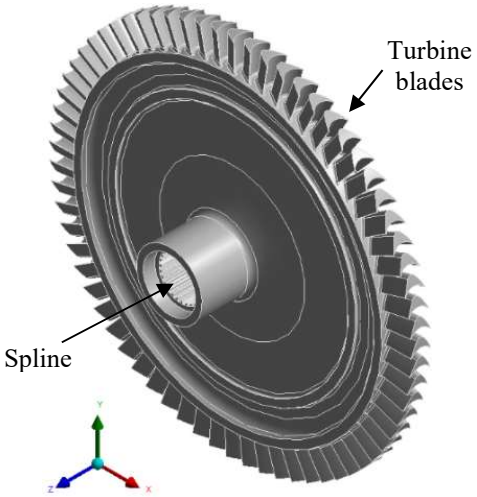

Figure 2. Turbine rotor 3D Model

2 Requirements

The L75 turbopump turbine rotor is a nickel-based superalloy blisk (blades and disk in one part) of 250 mm diameter with 68 prismatic blades and a spline in the hub, as Zink [2]. The geometric model of the turbine rotor is shown in the Fig. 2.

The pressure and temperature distribution in the turbine blades are based on a CFD (Computational Fluid Dynamics) analysis performed in the context of the L75 turbopump development. The hot gas flows from gas generator and passes at supersonic velocity through the turbine blades, transfering part of its kinetic energy and creating pressure and temperature profiles on blade surfaces, as Sutton [7]. The difference of the pressures on the blade surfaces generates the torque which is driven to the shaft by a spline at the hub. The pressure and temperature distribution on the L75 blade surfaces can be observed in the Fig. 3. As it is a partial admission turbine, the hot gas flows only through a few blades at once, making the blades to be subjected to a stress cycle as the rotor turns.

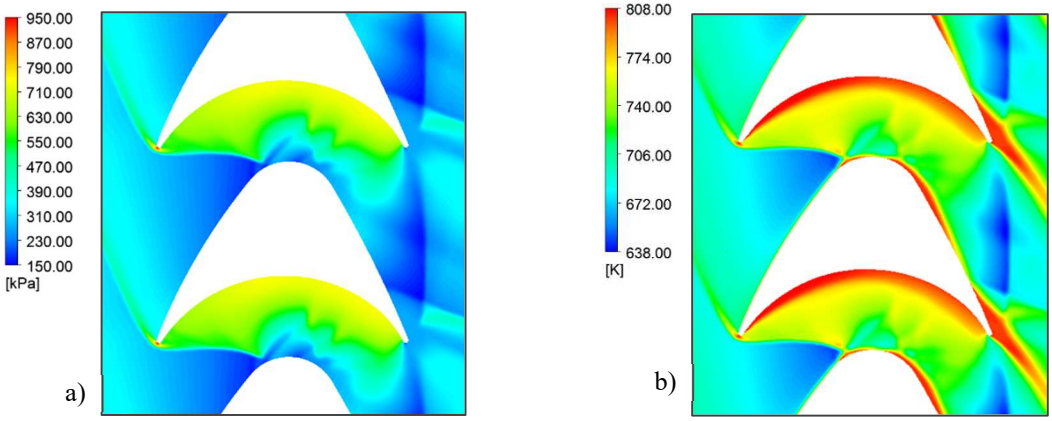

Figure 3. Static pressure (a) and temperature (b) of gas flow through the turbine blades.

The following requirements and operation conditions are considered in the turbine rotor analysis, based on the requirements defined in Almeida [1], Zink [2] and Pfuetzenreuter [5], and in the CFD analysis of turbine flow:

- Turbine rotor (blisk) material: Inconel 713-C cast nickel superalloy
- Rotational speed (max.): 27600 rpm
- Turbine torque (max.): 245 N.m
- Required lifetime: 4000 seg (1.11 hs)
- Number of starts: 10
- Gas pressure: disk: 315 kPa, blades: profile as CFD analysis
- Gas temperature: disk: 670 K, blades: profile as CFD analysis

The main turbine regions likely for failure are blade tip, blade roots, hub hole and hub spline, as Sims [6].

The main failure modes considered in this analysis, as defined based on Boyce [3] and Giampaolo [4] are:

1. Elastic deformation (it could lead the blade tip to rub the casing or increase the rotor unbalance)
2. Plastic deformation (it could increase the rotor unbalance or lead to rupture)
3. High-cycle fatigue (it could lead blade to crack due to vibration excited by blade/nozzle pass-by)
4. Low-cycle fatigue (it could cause cracks in disk and blade root due to blisk thermal cycling during start-stop operation

The elastic deformation has an additional impact on the turbine performance, since it must be compensated by increasing the blade tip gap to avoid rubbing the casing, as Boyce [3].

The safety factors considered in this analysis are based on european aerospace standards ECSS [8] and [9], as Almeida [1] and Pfuetzenreuter [5], and are defined as 1.2 for elastic deformation, 1.5 for plastic deformation and 2.0 for fatigue lifetime. In this study the conditions to approval are obtained by comparing the turbine rotor stress/strain distribution defined in this FEM analysis and the admissible values, which are calculated based on the material properties and the safety factors.

3 Structural Analysis

The aim of this structural analysis is to verify whether the turbine rotor can support the mechanical loads related to the turbine operation condition.

3.1 Material properties

The material properties of the turbine rotor used in this study are based on data in ASM International [10] and Zahnke [11] and are shown in the Tab. 1. As some properties are dependent of the temperature, the values are presented in function of temperature up to 540 ºC (813 K), which is the maximum temperature of the gas flow expected by the CFD analysis. The variation of the properties between these points can be considered linear. The fatigue properties shown in the Tab. 1 are defined considering the number of cycles during the blades' lifetime. Thus the number of stress cycles is defined by calculating the number of turns the turbine realizes during its lifetime, which is 2.10^6 in this case, and the number of thermal cycles is defined by the number of starts and stops the turbine performs in its lifetime, which is 10 in this case. In principle, the stress cycling brings the material into high cycle fatigue and the thermal cycling leads the material to low cycle fatigue, as Sims [6].

Table 1. Inconel 713-C properties

Temperature	Elastic Module	Poisson ratio.	Specific mass	Thermal Expansion	Thermal Conductivity	Yield Strength	Rupture Strength	Fatigue Strength*	Fatigue Strain**
ºC	GPa		Kg/m³	10^{-6} C	W/m.K	MPa	MPa	MPa	%
21	205	0,3	7910	10,1	9,9	740	850	280	2,2
540	180	0,3	7750	13,5	17,0	705	860	245	1,8

(*) Stress amplitude for failure in 2.10^6 cycles (high cycle fatigue)

(**) Strain amplitude for failure in 10 cycles (low cycle fatigue)

Considering the failure modes, the admissible stress values are calculated based on the safety factors defined

in Section 2 (1.2 for elastic deformation, 1.5 for plastic deformation and 2.0 for fatigue lifetime), the rotor material properties, and a manufacturing safety factor of 1.15 related to the physical and chemical heterogeneity of cast made materials. This is a design strategy adopted due to the large variation of material properties noticed in cast nickel alloy turbine parts, as Sims [6]. The admissible blade tip displacement is defined based on the dimensions of the rotor, the blade tip gap and a safety factor of 1.5 in order to avoid any contact between the blades and the casing. In this case the thermal expansion of the blade tip is not considered as it is already compensated by heating the casing. Therefore, the maximum admissible values for turbine rotor are defined in the Tab. 2.

Table 2. Admissible values for structural approval

Temperature	Elastic Stress	Plastic Stress	Blade Tip Displacement	High-cycle Fatigue Stress*	Low-cycle Fatigue Strain**
ºC	MPa	MPa	mm	MPa	%
21	535	495	1.25	280	2,1
540	510	500	0.65	245	1,8

(*) Stress amplitude for failure in 4.10^6 cycles (high cycle fatigue)

(**) Strain amplitude for failure in 20 cycles (low cycle fatigue)

3.2 FEM model

In order to reduce the simulation time some simplifications of turbine rotor model geometry are made, such as removing screws and holes (in low stress regions and with purpose only for assemble process). Furthermore, chamfers and radius are kept in the model to accurately reproduce the effects of local stress concentrations, as reccomended by Ansys [12].

The FEM mesh used for the structural analysis is relatively coarse in the disk, finer in the blades and in the hub and finest in the blades radius and in the spline teeth, since the aim is to obtain more accurate results in regions of stress concentration, as Reddy [13] and Bathe [14], which is shown in Fig. 4. The FEM model is obtained with about 1.1 million tetragonal (mainly) elements and about 1.5 million nodes using the software ANSYS® Workbench™ R.17.0 with modules SpaceClaim™ and Mechanical™.

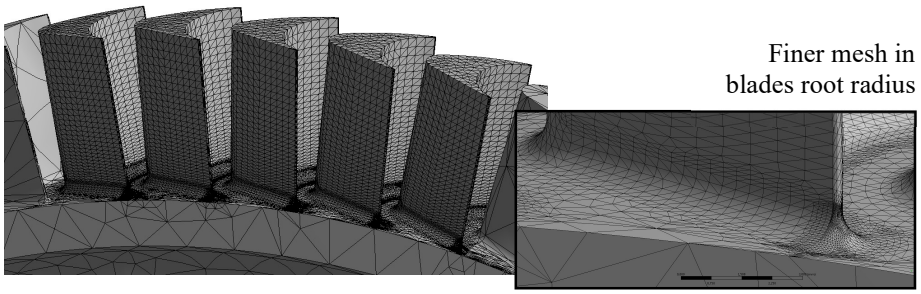

Figure 4. FEM model mesh in the turbine blades for structural analysis with blade root in detail.

3.3 Boundary Conditions

The FEM model is supported by slide type smooth restraints in cylindrical surfaces of the hub central hole and in the lateral surfaces of the spline teeth. A rotation speed of 27600 rpm is imposed in the turbine rotor (centrifugal acceleration load). The pressure and temperature distribution defined in the CFD analysis are applied in the blades and disk surfaces. For simplification it is considered the temperature of the rotor surfaces is the same as the hot gas (convection coefficient is considered infinite). Hence, it is imposed on the disk a pressure of 315 kPa and a temperature of 670 K, and it is imposed on the blade a pressure distribution from 150 to 950 kPa and a temperature distribution from 680 to 800 K, approximately. A smooth transition is considered in the regions next to the blade, such as the blade root radius and platform.

3.4 Results

For deformation failure modes the operational conditions of the turbine rotor are simulated, therefore it is considered the rotor is subjected to the temperature distribution, the rotational speed, and the pressure distribution in its surfaces. The von Mises stress distribution in the rotor is presented in Fig. 5. It can be noted the maximum stress is 488 MPa and occurs in the blade root radius region, which is less than the admissible value for any temperature for deformation failures, as Tab. 2. It is also observed that the stress values in the spline teeth are lower than the blades. The Fig. 6 shows the displacement at the same conditions above. The effect of thermal expansion in the displacement was hidden in this result. It is noted the maximum displacement occurs in the blade tip and the value (0.11 mm) is less than the maximum admissible value for this location, as Tab. 2.

For fatigue failure modes, only the alternative loads are applied in the FEM model to determine the amplitude of the stress which the material is subjected to. In the case of the low cycle fatigue the rotor is subjected to all operation conditions any time the turbine is started and put in operation, thus considering the condition above, the strain of the rotor material during operation condition is shown in the Fig.7. It is noted that the maximum strain is 0.24 % and occur in the blades root region, therefore it is less than the maximum admissible value for fatigue failure, as Tab. 2. Furthermore, in the case of the high cycle fatigue the turbine blades are subjected to alternative load by hot gas flow at every time they pass through the nozzle, thus considering only the gas flow pressure, the stress due to this condition is shown in the Fig. 8. It is noted that the maximum stress is 120 MPa, which is less than the maximum admissible value for fatigue failure defined in the Tab. 2.

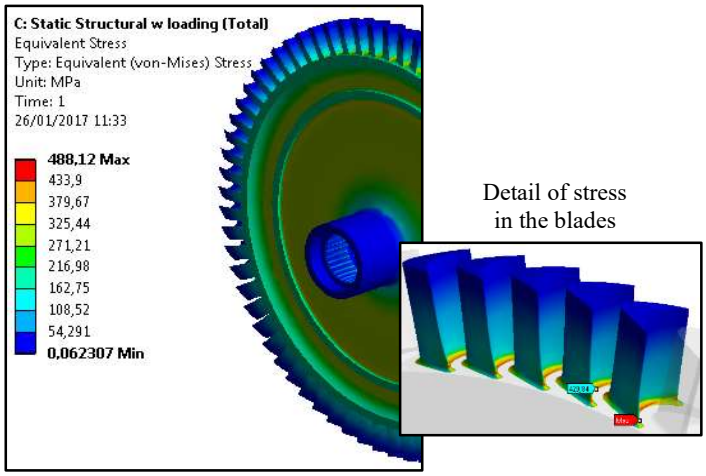

Figure 5. Stresses (von Mises) in the turbine rotor at the operation conditions with blades in detail.

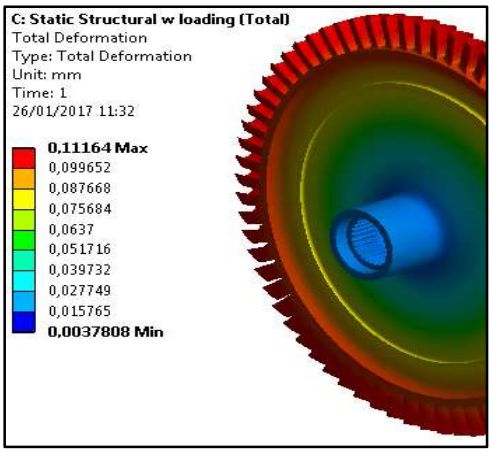

Figure 6. Displacement of the turbine rotor at the operation conditions.

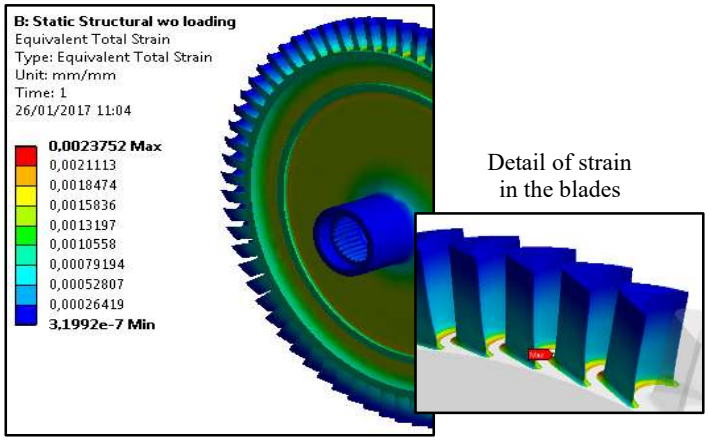

Figure 7. Strain in the turbine rotor at the operation condition with blades in detail.

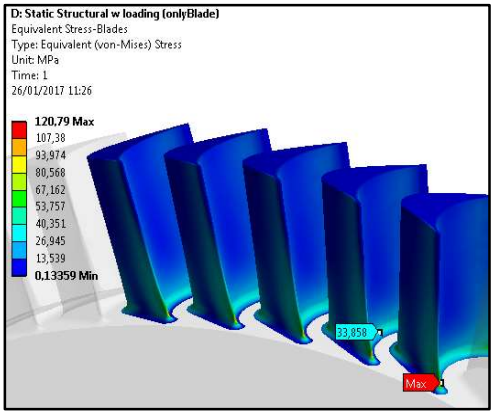

Figure 8. Stress (von Mises) in the turbine blades at only the gas flow pressure.

In summary, as the results presented above, the turbine rotor is approved in the structural analysis with a small margin related to the plastic deformation failure mode. The rotor design would be more robust if the material has better plastic properties and/or the blade root radius was improved.

4 Modal Analysis

The aim of this modal analysis is to verify the resonance conditions by comparing the natural frequencies of the turbine rotor with the frequency of variation of the loads which the rotor is exposed to. If the condition of resonance is identified the alternative force could be amplified by the rotor and it could experience failure by vibration. Although presenting great influence, as Lima [15], the bearing behavior is not simulated in this analysis.

4.1 FEM model

The FEM model is the same as used in the structural analysis with the exception of the mesh size. For the modal analysis the distribution of elements is relatively homogeneous along the rotor in order to maintain the mass balance, as Sias [16]. This FEM model mesh is made of about 1 million elements and 1.4 million nodes. The boundary conditions of the FEM model, i.e. the restraints and loads, are the same as those of the structural analysis, as the natural frequencies are dependent of the temperature and stress of the material. Therefore, the initial condition for modal analysis is the operation condition defined in the structural analysis.

The failure mode by vibration is defined by the coincidence of any of the first natural frequencies of the rotor with the frequency which the blades pass through the gas flow from nozzle, or the first multiples of it. Thus, considering the rotational speed, the frequency of the blade passing-by is 460 Hz.

The 10 first rotor natural frequencies obtained by FEM analysis are presented in Tab. 3. The first mode should not be considered as it is an effect of a restraint limitation of the FEM model. It is noted that there are no coincidences between the rotor first natural frequencies and the blades passing-by frequency or its 8 first multiples.

Table 3. Natural frequencies of turbine rotor

Mode.	1	2	3	4	5	6	7	8	9	10
Freq. (Hz)	0.005	615.1	724.2	1097	1145	1578	2058	2265	3342	3410

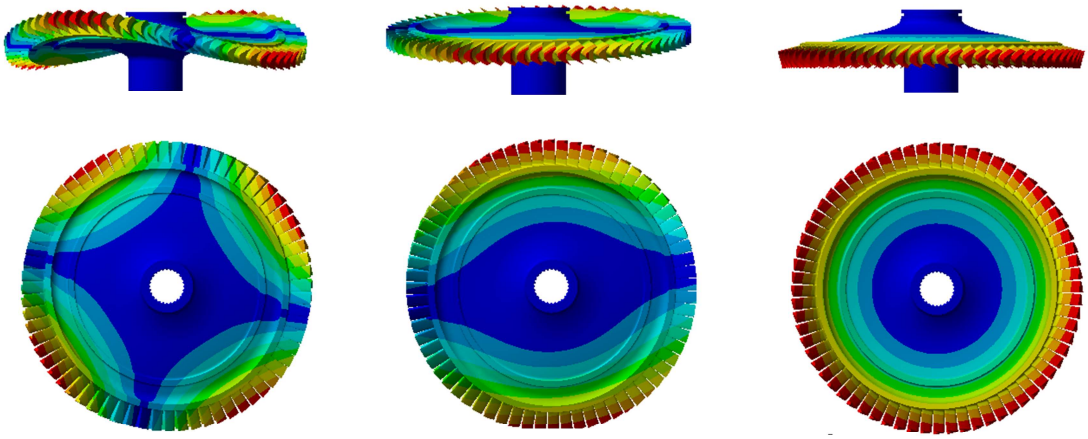

(a) Vibration Mode 2 (b) Vibration Mode 3 (c) Vibration Mode 5

Figure 9. Main rotor vibration modes: displacement aspect.

The more relevant vibration modes are shown in the Fig. 9, where the geometry of the vibration movement can be seen. It can be observed that the vibration modes 2 and 3 would be more critical for failure if their frequencies were coincident with any first multiples of blades passing-by frequency. On the other hand, the rotor design would be more robust if the natural frequencies of the mode 2 and 3 were higher than 2 times the blades passing-by frequency (920 Hz), which could be obtained improving the disk thickness a few millimeters.

In summary, as the results presented above, the turbine rotor is approved in the modal analysis. Furthermore, a more robust design could be obtained by increasing the disk thickness.

5 Conclusions

The modal and structural analysis demonstrate the turbine rotor is able to support the operating conditions with a small margin. The most likely failure mode is the plastic deformation. It was expected as the rotor is made by a cast material, which has poor plastic properties.

A more robust design would be obtained if the material had better plastic properties, such as a forged nickel superalloy, as the singular creep properties of the Inconel 713-C are not even needed in this design. An improving of the blade root radius could also make the rotor design more robust, as it is the most stressed region. Additionally, the rotor would be less susceptible to vibration resonance during operation if the turbine disk thickness was slightly increased. Taking to account that a plastic deformation or a vibration resonance could lead the turbine rotor to a catastrophic failure, the IAE's turbopump development team decided, based on this study, to perform a risk analysis and a design review of the L75 turbine.

Acknowledgements. The authors wish to thank AEB/IAE for supporting all activities performed in the frame of the L75 project and to thank CAPES (PROAP) for supporting the publication of this work.

Authorship statement. The authors hereby confirm that they are the sole liable persons responsible for the authorship of this work, and that all material that has been herein included as part of the present paper is either the property (and authorship) of the authors, or has the permission of the owners to be included here.

References

[1] D.S. Almeida, C.M.M. Pagliuco. "Development status of L75: A Brazilian liquid propellant rocket engine". *Journal of Aerospace Technology and Management 6(4)*, pp.475-484. 2014.
[2] E.S. Zink, D. Bourdon, D.S. Almeida, Pagliuco CMM, Wagner B, Kitsche W, Langel G. "Biofuel turbopump development strategy: L75 Liquid oxygen and ethanol engine case". *53rd AIAA/ASME/SAE/ASEE Joint Propulsion Conference*, AIAA 2017-4929; Atlanta, USA, 2017.
[3] M.P. Boyce. *Gas Turbine Engineering Handbook*. 2nd ed. Gulf Professional Pub. USA, 2002.
[4] T. Giampaolo. *The Gas Turbine Handbook: Principles and Practices*. 2nd ed. Fairmont Press. USA, 2003
[5] L. Pfuetzenreuter, H. Burkhardt, B. Wagner, D.S. Almeida, C.M.M. Pagliuco, L.B. Nascimento, B.R.D. Souza. E.S. Zink, T.B. Araujo, et al. "L75 LOx Ethanol Engine: Current Status of Thrust Chamber and Turbopump Cooperative Development". *53rd AIAA/SAE/ASEE Joint Propulsion Conference*. AIAA 2017-4929. Atlanta, USA, 2017.
[6] C.T. Sims, N.S. Stoloff, W.C. Hagel. *Superalloys II*. Wiley-Interscience. USA, 1986.
[7] G.P. Sutton. "History of Liquid Propellant Rocket Engines". *American Institute of Aeronautics and Astronautics, Inc*. 911 p. Virginia, USA. 2006.
[8] ECSS - European Cooperation for Space Standardization. *ECSS-E-30 part 5.2 rev.1: Propulsion for Launchers – Solid and Liquid*. 2004.
[9] ECSS - European Cooperation for Space Standardization. *ECSS-M-ST-10C: Project planning and implementation*. 2009.
[10] ASM International. *ASM Handbook vol.1 – Properties and Selection*. The Material Information Company. USA, 1990.
[11] R. Zahnke. *Aerospace Structural Metals Handbook*. Cindas LLC/Purdue University. 2007.
[12] Ansys. *ANSYS® Mechanical™ Tutorial*, ANSYS Workbench Release 17.0, 2016.
[13] J.N. Reddy. *Introduction to the Finite Element Method*, 4th. ed., McGraw Hill, 2018.
[14] K.J. Bathe. *Finite Element Procedures*, 2nd Ed., 2014.
[15] S.F.P. Lima, C.A. Souto. "Dynamic Modeling of a Liquid Rocket Engine Turbo Pump Rotor". *Proceedings of the XLI Ibero-Latin-American Congress on Computational Methods in Engineering, ABMEC*. Foz do Iguaçu, PR, Brazil. 2020.
[16] D.F. Sias, E. Barros, C.A. Souto, D.S. Almeida. "Dynamic Analysis of a Liquid Rocket Turbopump Unit". *23rd ABCM International Congress of Mechanical Engineering*. COBEM 2015. Rio de Janeiro, RJ, Brazil, 2015.